This document is the Accepted Manuscript version of a Published Work that appeared in final form in **ACS Applied Polymer Materials**, copyright 2022 American Chemical Society after peer review and technical editing by the publisher. To access the final edited and published work see https://pubs.acs.org/doi/10.1021/acsapm.2c00839

Jasinska-Walc L., Duchateau R., Defize T., Bouyahyi M., Rozanski A., Yang L., Patham B., Sweere T., Hochstädt S., Hansen M. R., Bernaerts K., Self-Organization of Graft Copolymers and Retortable iPP-Based Nanoporous Films Thereof, ACS Applied Polymer Materials (2022), DOI: 10.1021/acsapm.2c00839

Self-organization of Graft Copolymers and Retortable iPP-based Nanoporous Membranes Thereof

Thomas Defize,[a] Miloud Bouyahyi,[b] Artur Rozanski,[c] Lanti Yang,[d] Bhaskar Patham,[e] Teun Sweere,[f] Sebastian Hochstädt,[g] Michael Ryan Hansen,[g] Katrien Bernaerts,[a] Lidia Jasinska-Walc,[h,b,] and Rob Duchateau[b,i,*]*

[a]Department of Biobased Materials, Maastricht University, P.O. Box 616, 6200MD Maastricht, the Netherlands

[b]SABIC Technology & Innovation, STC Geleen, Urmonderbaan 22, Geleen, The Netherlands

[c]Centre of Molecular and Macromolecular Studies, Polish Academy of Sciences, Sienkiewicza 112, 90-363 Lodz, Poland

[d]SABIC Technology & Innovation, Plasticslaan 1, 4612 PX, Bergen op Zoom, The Netherlands

[e]SABIC R&T India, Village: Chikkadunnasandra, Anekal: Taluk, Off. Sarjapura - Attibele State Highway State Highway, Bengaluru, 562125

[f]Siemens Industry Software Netherlands B.V., Galileiweg 8, 2333 BD Leiden, The Netherlands

Classification: Internal Use

[g]Westfalische Wilhelms-Universitat Munster, Institut fur Physikalische Chemie, Corrensstr. 28/30, 48149 Munster, Germany

[h]Department of Chemistry and Technology of Functional Materials, Gdansk University of Technology, G. Narutowicza Str. 11/12, 80-233 Gdansk, Poland

[i]Chemical Product Engineering, Department of Chemical Engineering, University of Groningen, Nijenborgh 4, 9747 AG Groningen, The Netherlands

Keywords: nanoporous membranes, polypropylene, graft copolymers, self-assembling, morphology

Abstract: Polyolefins might become inexpensive alternatives to the existing membranes based on polyethersulfone. Here we disclose the production of retortable, well-defined PP-based nanoporous membranes derived from amphiphilic graft copolymer precursors. The graft copolymers, containing a polypropylene backbone and polyester grafts, were obtained by grafting lactones, specifically δ-valerolactone and ε-caprolactone, from well-defined randomly functionalized poly(propylene-*co*-10-undecen-1-ol) as a macroinitiator. Depending on the composition, the graft copolymers self-assemble into droplet, cylindrical, lamellar or interconnected two-phase morphologies. Functional mesoporous iPP-based membranes were fabricated by the selective degradation of the polyester blocks of the copolymers. Their structure and morphology were studied using AFM, SEM and SAXS and solid state NMR, while the mesoporosity was assessed by nitrogen sorption experiments. The pore size of the membranes is strongly influenced not only by the volume fraction of the copolymer blocks but unexpectedly also

MOST WIEDZY Downloaded from mostwiedzy.pl

Classification: Internal Use

by the topology (i.e. number of grafts) of the graft copolymer, as was confirmed by computational modeling studies using the Dynamic Density Functional Theory (DDFT) engine within the Culgi software. This work provides a conclusive answer on how the morphology of iPP-based graft copolymers is tuned by the copolymer composition and the amount and length of the grafted polyester blocks. Filtration tests and flux determination demonstrated that such structurally-well defined mesoporous products can be successfully applied for ultrafiltration processes while the chemical resistance- and sterilization tests revealed their robust performance and suitability for water purification applications.

Introduction

Emerging technologies using polymer-derived nanoporous membranes reveal a high potential for a wide range of applications such as medicine, water purification and industrial separation processes.[1] Owing to the facile processability of polymers, tunability of the pore size and low costs of the corresponding membranes compared to ceramics, polymeric membranes for controlled separation find use in various areas from water purification to biomedical applications. Currently, commercially available membranes are mainly fabricated from poly(vinylidene difluoride), poly(ethylene-co-chlorotrifluoro-ethylene), polysulfone, polyethersulfone, polyphenylsulfone or aromatic polyamides. The processing conditions of polymeric membranes viz. molecular imprinting,[2] controlled foaming,[3] controlled crazing[4], temperature and nonsolvent-induced phase separation (NIPS),[5-11] self-assembly and nonsolvent-induced phase separation (SNIPS)[12-16] or selective degradation of block copolymers[17-26] critically affect their morphology, properties and thus application area. Due to the relative simplicity to alter the chemical composition of block

MOST WIEDZY Downloaded from mostwiedzy.pl

Classification: Internal Use

copolymers, they are receiving increasing interest for the production of membranes with tunable pore size and mechanical properties.

The first efficient strategy for the synthesis of well-defined block copolymers and analysis of their complex architectures has been reported by Szwarc.[27] These polymers, consisting of immiscible blocks, self-assemble into ordered morphologies at the mesoscopic scale, which depends mostly on the overall degree of polymerization, the volume fraction of each segment and the segment-segment (Flory-Huggins) interaction parameters. Matsen and Bates[28] have extensively studied the properties of block copolymers to understand and predict their self-assembly into ordered structures. Importantly, these block polymers can serve a broad range of applications such as vesicles,[29] polyelectrolytes[30,31] or other nanostructured materials with enhanced mechanical properties.[32-35]

Block copolymers are also suitable precursors for the preparation of nano- or mesoporous materials with ordered morphologies via selective block sacrifice of cylindrical or bicontinuous morphology. This route was presented for the first time by Nakahama and coworkers,[36] who generated nanopores in a polystyrene matrix by selective degradation via ozonolysis of polyisoprene sequences in a cross-linked polystyrene-polyisoprene block copolymer. As presented by Hillmyer and coworkers,[37] PLA was successfully used as sacrificed block to produce either polystyrene or hydrogenated polybutadiene-based nanoporous membranes.[38,39] Other researchers produced similar PE-*block*-PLA copolymers starting from chain-end functionalized polyethylene produced by coordinative chain transfer polymerization followed by air oxidation.[40,41] The latter research groups have done a great job demonstrating the potential of producing polyolefinic membranes and starting from amphiphilic polyolefin-based block copolymers. Authors explained that starting from hydrogenated polybutadienes is rather expensive and the oxidation of

MOST WIEDZY Downloaded from mostwiedzy.pl

Classification: Internal Use

polyethylenes to hydroxyl chain-end functionalized polyethylenes, using coordinative chain transfer polymerization, generally does not exceed 80 % efficiency. Furthermore, the melting point of polyethylene-based membranes is too low to allow standard sterilizations methods.

Herein we describe the synthesis of iPP-based mesoporous membranes exhibiting tunable pore sizes, via the self-assembly of iPP-*graft*-polyester copolymers (Scheme 1) followed by selective etching of the polyester blocks and performance testing of the produced membranes. Using randomly functionalized-, rather than chain-end functionalized, polypropylene assured that a larger fraction of the polypropylene chains was functionalized and allowed us to vary the average number of polyester branches in the final graft copolymers. It was anticipated that the topology of the graft copolymers might influence the self assembly process and final morphology. The simulations of the microphase separation of the various graft copolymers, revealing different chemical composition and topology, were performed by the Dynamic Density Functional Theory (DDFT) engine within the Culgi software. The simulations demonstrated that the morphologies can be well predicted based on the molecular composition of the graft copolymers.

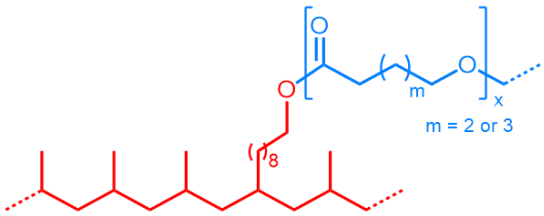

Scheme 1. Chemical structure of the copolymers used for the iPP-based nanoporous membrane preparation.

Experimental Section

Materials. δ-Valerolactone (VL; 98%, TCI) ε-caprolactone (CL; 97%, Sigma-Aldrich) were dried over CaH_2 (95 %, Sigma-Aldrich) and distilled under reduced pressure. Diethyl ether was used as

MOST WIEDZY Downloaded from mostwiedzy.pl

Classification: Internal Use

received. Toluene (anhydrous, Sigma-Aldrich) was purified using an MBraun-SPS-800 purification column system and was stored on 4-Å molecular sieves under an inert atmosphere before use. 10-undecen-1-ol was purchased from Sigma Aldrich, distilled under reduced pressure and stored on 4-Å molecular sieves under an inert atmosphere. Methylaluminoxane (MAO) (30 wt. % solution in toluene) was purchased from Chemtura. Diethylzinc (DEZ) (1.0 M solution in hexanes), triisobutylaluminum (TiBA) (1.0 M solution in hexanes) were purchased from Sigma Aldrich. *rac*-$Me_2Si(2\text{-}Me\text{-}4\text{-}Ph\text{-}Ind)_2ZrCl_2$ was purchased from MCAT GmbH, Konstanz, Germany. Isotactic polypropylene (*i*-PP) (SABIC - PP520P, MFR = 10.5 g·10 min^{-1} (230 °C, 2.16 kg)), tin(II) 2-ethylhexanoate ($Sn(Oct)_2$) (92 – 100 %, Sigma-Aldrich), titanium (IV) n-butoxide ($Ti(OBu)_4$, Sigma Aldrich), Irganox 1010 (antioxidant, BASF) were used as received. 3-aminopropyl functionalized silica nanoparticles (3 % (w/v) in ethanol) were purchased from Sigma-Aldrich.

Synthesis of poly(propylene-*co*-10-undecen-1-ol) (iPP-OH). The propylene – 10-undecen-1-ol copolymerization was carried out in a stainless steel Büchi reactor (300 mL). Prior to the polymerization, the reactor was dried in vacuo and flushed with nitrogen. Toluene (100 mL) was introduced into the reactor followed by TiBA (1.0 M solution in hexane, 5 mL) and the functionalized comonomer (10-unedecen-1-ol; 1 mL, 2.5 mmol) under a nitrogen atmosphere (1 bar). The resulting solution was stirred for 15 – 20 min. Subsequently MAO (30 wt% solution in toluene, 2.0 mL) was introduced into the reactor under nitrogen atmosphere after which the solution was saturated with propylene (5 bar total pressure). In a glovebox, a stock solution of *rac*-$Me_2Si(2\text{-}Me\text{-}4\text{-}Ph\text{-}Ind)_2ZrCl_2$ (5 mg, 8 μmol) in toluene (10 mL) was prepared and the catalyst solution (5 mL) was transferred into the reactor using over pressure of nitrogen atmosphere (1 bar). The propylene pressure was maintained constant for 30 min. At the end of the polymerization

MOST WIEDZY Downloaded from mostwiedzy.pl

Classification: Internal Use

reaction, the propylene feed was stopped and the residual propylene was released from the reactor. The resulting mixture was quenched in acidified methanol (300 mL, 2.5 wt% of concentrated HCl), filtered and washed with demineralized water. The obtained powder was dried in a vacuum oven under reduced pressure at 60 °C overnight.

Synthesis of PP-*graft*-PCL via catalytic ring-opening polymerization. iPP-OH (4 g, M_n = 27.8 kg·mol^{-1}, $Đ$ = 2.3) was placed in a round bottom flask with a magnetic stirrer and dried by Dean-Stark distillation in toluene (100 mL) for 24 h. The solution was cooled to 100 °C and catalyst $Sn(Oct)_2$ (180 mg, 0.44 μmol) and ε-caprolactone (10.27 g, 89.9 mmol) were added. The ring-opening polymerization reaction was carried out for 24 h under inert atmosphere. The progress of the copolymerization was followed by ^{1}H NMR spectroscopy by taking aliquots at set time intervals. The synthesized copolymer was isolated by the precipitation in diethyl ether and dried in a vacuum oven at 40 °C for 24 h. Yield: 94 %.

Synthesis of PP-*graft*-PVL via catalytic ring-opening polymerization. iPP-OH (4 g, M_n = 27.8 kg·mol^{-1}, $Đ$ = 2.3) was placed in a round bottom flask with a magnetic stirrer and dried by Dean-Stark distillation in toluene (100 mL) for 24 h. The solution was cooled down to 100 °C and catalyst $Sn(Oct)_2$ (180 mg, 0.44 μmol) and δ-valerolactone (10.00 g, 100 mmol) were added. The reaction was carried out for 24 h under inert atmosphere. The progress of the copolymerization was followed by ^{1}H NMR spectroscopy by taking aliquots at set time intervals. The synthesized copolymer was isolated by the precipitation in diethyl ether and dried in a vacuum oven at 40 °C for 24 h. Yield: 95 %.

Compression molding. All the copolymer-based films were prepared via compression molding using PP ISO settings on a LabEcon 600 high-temperature press (Fontijne Presses, the Netherlands). The copolymers were introduced into a Teflon mold to prepare samples with a

MOST WIEDZY Downloaded from mostwiedzy.pl

Classification: Internal Use

thickness of 0.18 mm. The program for the compression molding involved the following steps: heating to 200 °C for 5 min at 5 bar followed by cooling to room temperature for 10 min at 5 bar.

Mesoporous membranes preparation. The degradation of the polyester blocks of the copolymers was carried out by immersing pieces of the PP-*graft*-polyester copolymer films in a 0.5 M solution of NaOH in a mixture of water and methanol (60:40 v/v). The solution was kept at 70 °C during 3 days and the porous membranes were then washed with slightly acidic MeOH (aq.) and MeOH and dried for 24 h under reduced pressure.

Membrane filtration procedure. The porous membrane was clamped into a glass filter device. Then vacuum was applied (20 mbar) and water was added at the top of the filtration device. The volumetric flux was calculated using the Equation 1

$$J_V = \frac{V}{A \cdot t} \quad (1)$$

where J_V is the volumetric flux, V is the volume (L), A is the area of the membrane (m^2) and t is the time (h). A filtration experiment was carried out using a dispersion of silica nanoparticles (3 % w/v in ethanol). The dispersion was filtrated using the same filtration setup and DLS experiments were carried out on the solutions before and after filtration.

^{1}H NMR spectroscopy. Liquid-state ^{1}H NMR spectra were recorded at 80 °C using a Varian Mercury Vx spectrometer operating at Larmor frequencies of 400 MHz. For the experiments, the spectral width was 6402.0 Hz, acquisition time 1.998 s and the number of recorded scans equal to 64.

Size Exclusion Chromatography (SEC). M_n, M_w and the polydispersity index (PDI, $Đ_M$) were determined using SEC. The measurements were performed at 150 °C on a Polymer Char GPC-IR® built around an Agilent GC oven model 7890, equipped with an autosampler and the Integrated

MOST WIEDZY Downloaded from mostwiedzy.pl

Classification: Internal Use

Detector IR4. 1,2-dichlorobenzene (oDCB) was used as an eluent at a flow rate of 1 mL·min^{-1}. The SEC-data were processed using Calculations Software GPC One®.

Differential Scanning Calorimetry (DSC) analysis. Melting (T_m) and crystallization (T_c) temperatures as well as enthalpies of the transitions were measured by DSC using a DSC Q100 from TA Instruments. The measurements were carried out at a heating and cooling rate of 10 °C·min^{-1} from −60 °C to 210 °C. The transitions were deduced from the second heating and cooling curves.

Sample preparation for Atomic Force Microscopy (AFM). For spin-coated self-assembled copolymer film, AFM imaging was directly performed on the film surface at ambient conditions without further treatment of the sample. For compression molding films imaging, the cross-section of films before and after degradation was used. The samples were cut into proper specimens and subsequently cryo-microtomed at –120 °C using microtoming equipment (LEICA EM UC7). A diamond knife (Diatome) mounted in a stainless steel holder was used to microtome the samples. Such cross-sectioned blocks were used for AFM measurements without further treatment.

Atomic Force Microscopy (AFM) analysis. AFM imaging was performed at Dimension FastScan AFM system from Bruker utilizing tapping mode AFM tips (Model TESPA-V2, k: 42 N·m^{-1}, f: 320 kHz). The software Nanoscope Analysis 1.5 from Bruker was used as the computer interface for operation and analysis of AFM measurements. All AFM measurements were performed at ambient conditions. Height and phase images were recorded simultaneously at a scan rate of 1 Hz with a resolution of 512 × 512 pixels. Optical imaging integrated in the AFM setup was first used before AFM measurement to select the area of interest for imaging.

Field Emission Scanning Electron Microscopy (FE-SEM) imaging. The cross-section morphology of the degraded self-assembled copolymer film was characterized by FE-SEM imaging (JEOL

MOST WIEDZY Downloaded from mostwiedzy.pl

Classification: Internal Use

JSM 7800-F) at an operation voltage of 5 kV using LED detector. To obtain an adequate contrast of the membrane nanopore morphology and to avoid destroying of the cross-sections of the membrane film, the samples for FE-SEM imaging were first immersed in liquid nitrogen, fractured and then sputtered with platinum/palladium (Pt/Pd).

Small-Angle X-ray Scattering (SAXS). The structure of the membranes was probed using 2-dimensional small angle X-ray scattering. The Kiessig-type camera with sample detector distance of 1.2 m was coupled to an X-ray CuK a low divergence microsource, operating at 50 kV and 1 mA (GeniX Cu-LD by Xenocs, France). The scattering produced by the sample was recorded with the Pilatus 100 K solid-state area detector of the resolution of 172 × 172 μm^2 (Dectris, Switzerland). Dimension of scattering objects was determined from one dimensional sections of 2-D pattern. Background and Lorentz corrections were applied to the curves. Dimension of scattering objects was then calculated from position of the maximum of corrected curves using the Braggs law.

The nitrogen adsorption–desorption analysis. The isotherms were measured at –196 °C using a Micromeritics ASAP 2420 analyzer. The samples were degassed overnight at 30 °C under high vacuum (133 Pa) prior to measurements. The specific surface area of the membranes was calculated using the Brunauer–Emmett–Teller method,[42] while the pore-size distribution was determined using the Barret–Joyner–Halenda model.[43]

Dynamic mechanical thermal analysis (DMTA). The experiments were performed using a TA Instruments Q800 DMA. Samples were tested by strain-controlled temperature ramp with the frequency of 1 Hz. The temperature profile was from −100 °C until the melting point of the polyolefin block with the ramp 3 $°C \cdot min^{-1}$. The glass transition temperature was estimated as the peak of the tangent delta signal.

MOST WIEDZY Downloaded from mostwiedzy.pl

Classification: Internal Use

Tensile tests. Mechanical properties were characterized by performing tensile test experiments in triplicate using a microtensile tester (Linkam, TST 350). Both ends of the tensile specimen (length: 30 mm, width: 2 mm, thickness: 0.18 mm) were gripped by jaws which were 15 mm apart. A load cell with a capacity of 200 N was used to measure the applied force. The tensile tests were carried out at a constant speed of 50 $\mu m \cdot s^{-1}$ at room temperature.

Dynamic Density Functional Theory (DDFT) studies. To predict the self-assembly of the investigated copolymers the Dynamic Density Functional Theory (DDFT) engine[44] within the Culgi software was used. The mesophase morphologies of various iPP-*graft*-polyester and iPP-*block*-polyester copolymer architectures have been investigated. Within DDFT, polymers are described by chains of soft and connected blobs. The molecular weight of blobs representing iPP was 1236 $g \cdot mol^{-1}$ and the molecular weight of blobs representing PVL and PCL was 1492 $g \cdot mol^{-1}$. The simulations were performed on a cubic box with an edge length of 100 nm containing 10000 iPP-polyester copolymers.[45-48]

Solid state NMR analysis. All samples were annealed for 30 minutes at 150 °C under N_2 atmosphere and cooled to room temperature at a rate of 10 K/min prior to solid-state NMR measurements. The solid-state $^{13}C\{^1H\}$ MAS NMR experiments were carried out on a Bruker Avance III 300 spectrometer ($\upsilon_L(^1H)$ = 300.XX MHz, 7.05 T) using a Bruker 4.0 mm H/X WVT double-resonance probe. The samples were packed in a 4.0 mm ZrO_2 rotor and sealed with a Vespel© top-cap. All spectra were recorded at a MAS frequency of 10.0 kHz at variable temperatures controlled using a Bruker VT 3000 temperature control unit. Calibration of the temperature was carried out using ^{207}Pb referenced to the absolute chemical shift of ethylene glycol.[49] ^{13}C chemical shifts and radio-frequency (rf) field strengths were calibrated using adamantane ($\delta(^{13}C)$ = 38.5 ppm/29.5 ppm) as secondary reference.[50] Calibration of the magic angle

MOST WIEDZY Downloaded from mostwiedzy.pl

Classification: Internal Use

was performed using $^{23}NaNO_3$. Typical experimental parameters for the CP-RINEPT experiments[51] were ^{1}H 90° pulses of 4 µs (υ_{rf} = 62.5 kHz) and ^{13}C 90° pulses of 5 µs (υ_{rf} = 62.5 kHz) using an inter-pulse delay of $1/(4*{}^{1}J_{CH})$ ($^{1}J_{CH}$ = 150 Hz) for the INEPT-block and a refocusing delay of $1/(3*{}^{1}J_{CH})$. A cross-polarization (CP) contact time of 3.0 ms with a ramp from 70 % to 100 % on the ^{13}C channel was used. Proton decoupling was employed using the SW_fTPPM[50] scheme with υ_{rf} = 62.5 kHz coupling strength during CP acquisition and υ_{rf} = 25.0 kHz during INEPT acquisition.[51] All experiments were conducted using a recycle delay of 6 s and 1200 scans. Processing, data analysis, and plotting was carried out using the Bruker Topspin 4.1.1 software and OriginPro2020b.

Sterilization tests. Steam sterilization experiments were performed in a gravity displacement autoclave using standard conditions (30 minutes at 121 °C).

Results and Discussion

Poly(propylene-*co*-10-undecen-1-ol)s (poly(C_3-*co*-C_{11}OH)) were obtained in good yields with tunable molecular weights and functionality levels by the copolymerization of propylene and TiBA-pacified 10-undecen-1-ol. These randomly hydroxyl-functionalized copolymers were used as macroinitiators for the catalytic ring-opening polymerization of δ-valerolactone (VL) or ε-caprolactone (CL) to produce the corresponding polypropylene-*graft*-poly(δ-valerolactone) (iPP-*g*-PVL) and polypropylene-*graft*-poly(ε-caprolactone) (iPP-*g*-PCL), respectively (Scheme 1). The graft copolymers topologies were modelled using coarse-grained modelling software (Culgi) (Scheme S1). The polymerizations were mediated by two different poly(C_3-*co*-C_{11}OH) samples having on average 3 OH groups per polymer chain and revealing M_n = 22.9 kg·mol^{-1}, $Đ$ = 2.6 (entry 1-3, 6, Table 1) or poly(C_3-*co*-C_{11}OH) with 6 OH groups per polymer chain and M_n = 27.8

MOST WIEDZY Downloaded from mostwiedzy.pl

Classification: Internal Use

kg·mol^{-1}, $Đ$ = 2.3 (entry 4-5, 7, Table 1), respectively. As presented in Table 1, the ring-opening polymerization of VL or CL initiated by poly(C_3-*co*-C_{11}OH) as macroinitiator was effective over a broad range of lactone/catalyst/macroinitiator ratios. Analysis of the graft copolymers by means of HT-SEC proved difficult due to the amphiphilic nature of the copolymers.[52,53] However, the chemical structure of the macroinitiators and resulting graft copolymers could successfully be elucidated by the ^{1}H NMR spectroscopy (Figure S1-S3). The spectrum, corresponding to the poly(C_3-*co*-C_{11}OH), displays the characteristic signal of α-$\underline{CH_2}$OH at 3.67 ppm. The formation of the iPP-based copolymers was clearly confirmed by the resonances at 3.79 ppm, 3.96 ppm and 4.09 ppm (Figure S1-S3). Based on the molecular weight of the poly(C_3-*co*-C_{11}OH) macroinitiators, the molecular weights of the graft copolymers were estimated by ^{1}H NMR spectroscopy (Table 1). The volume fractions of the polypropylene and polyester segments were calculated based on the corresponding molar fractions and intrinsic densities of the homopolymers (Table 1). A polypropylene volume fraction of 30 to 50 vol% in the graft copolymers was targeted as this was assumed to lead to the right morphology (cylindrical or interconnected two-phase morphology) necessary for subsequent membrane formation.

Table 1. Molecular characterization of PP-*g*-PVL and iPP-*g*-PCL copolymers.

Entry	Branches/ chain [a]	VL/CL/cat./init.	M_n [kg·mol^{-1}][b]	$Đ$ [b]	M_n, PVL/PCL [kg·mol^{-1}][c]	iPP/PVL/PCL [mol%][c]	iPP/PVL/PCL [vol%][c]
1	3	125/0/1/2	22.5	2.9	9.5	66/34/0	0.50/0.50/0
2	3	125/0/1/2	23.2	2.9	10.4	63/37/0	0.46/0.54/0
3	3	250/0/1/2	14.6	4.0	17.2	52/48/0	0.35/0.65/0
4	6	225/0/1/2	21.9	3.2	8.8	56/44/0	0.39/0.61/0

MOST WIEDZY Downloaded from mostwiedzy.pl

Classification: Internal Use

5	6	250/0/1/2	24.6	3.1	9.9	53/47/0	0.36/0.64/0
6	3	0/225/1/2	31.2	3.8	19.4	52/0/48	0.33/0/0.67
7	6	0/250/1/2	20.3	4.9	11.6	53/0/47	0.33/0/0.67

[a] Determined by ^{1}H NMR, [b] measured by HT-SEC in o-DCB at 150°C according to PS standards, [c] molecular weight, mol and volume fraction of PVL or PCL blocks determined by ^{1}H NMR.

The microphase separation of the graft copolymers' segments by self-assembly was studied by AFM on thin films prepared by compression molding at 200 °C for 5 min. Additionally, for better understanding of the various copolymer compositions morphologies, computational modeling studies were performed. It should be noted that under the applied annealing conditions the self-assembly of graft copolymer in the prepared films is probably not in the kinetic equilibrium state yet however, sufficient for the nanoporous membrane preparation. The cross-sectional AFM phase images of polypropylene-*graft*-polyester with a different volume fraction of the iPP and polyester blocks are presented in Figure 1 and Figure S4. The morphology of the graft copolymers changes significantly with changing polypropylene and polyester volume fractions. Whereas for the lower and upper range of the polypropylene volume fraction (e.g. 33–36 vol% and 48 vol%) an interconnected two phase morphology with one phase forming nano-domains was observed (Figure 1A, C, D). Interestingly the graft copolymers containing around 40 vol% polypropylene ($iPP_{39vol\%}$-*g*-$PVL_{61vol\%}$) exhibit a periodic lamellar self-assembly structure with a lamellae pitch size of around 25 nm (Figure 1B). As proven, the interconnected two-phase morphology with nano-domains is suitable for the production of nanoporous membranes by selective phase sacrification.

MOST WIEDZY Downloaded from mostwiedzy.pl

Classification: Internal Use

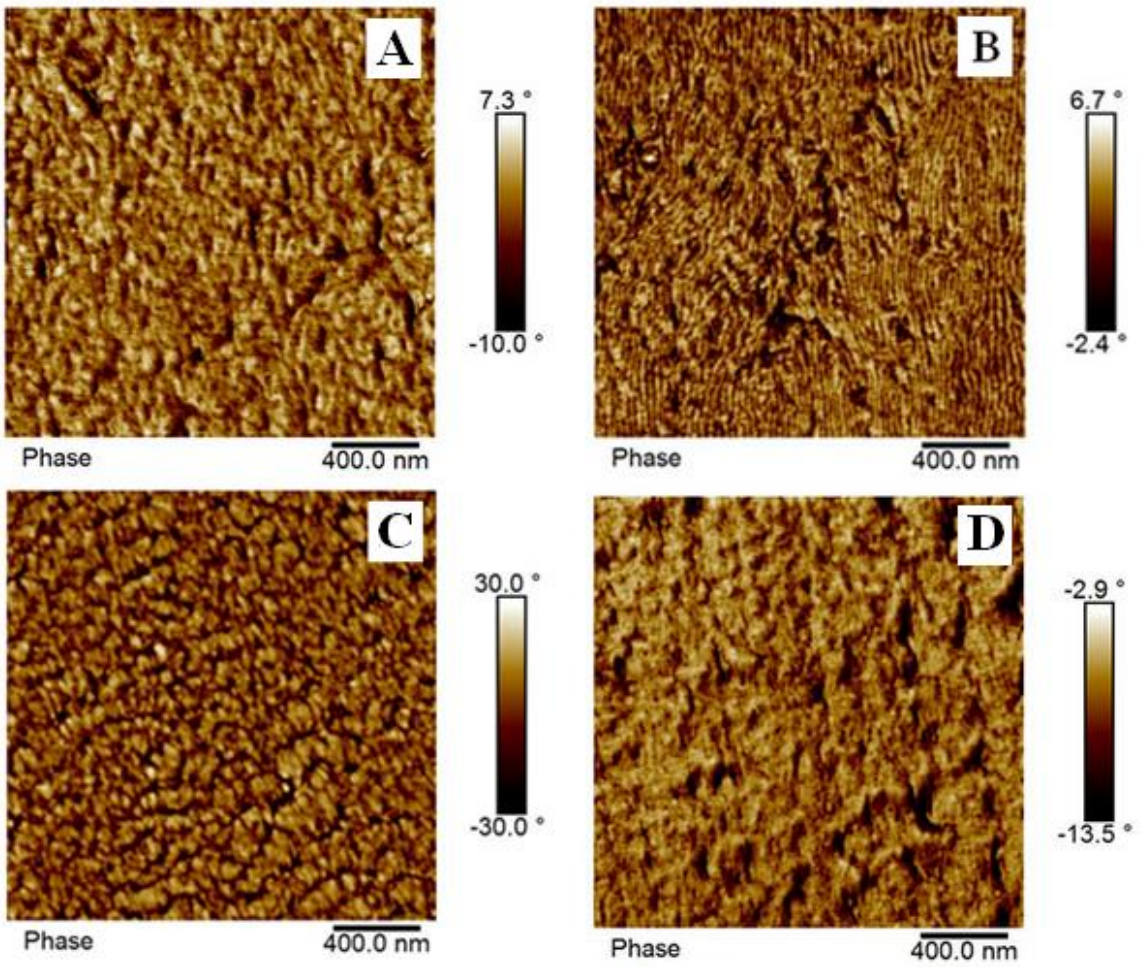

Figure 1: AFM phase images of iPP$_{46vol\%}$-*g*-PVL$_{54mol\%}$ (A, Table 1 entry 2), iPP$_{39vol\%}$-*g*-PVL$_{61vol\%}$ (B, Table 1, entry 4), iPP$_{36vol\%}$ -*g*-PVL$_{64vol\%}$ (C, Table 1, entry 5) and iPP$_{33vol\%}$-*g*-PCL$_{67vol\%}$ (D, Table 1, entry 6).

Variable temperature (VT) ^{13}C solid-state MAS NMR spectroscopy experiments were performed to gain insight into the structural properties and the temperature response of the graft copolymers. Heteronuclear cross polarization (CP) combined with refocused insensitive nuclei enhanced by polarization transfer (RINEPT) was carried out (referred to as CP-RINEPT)[51] on iPP$_{33vol\%}$-*g*-PCL$_{67vol\%}$ containing on average 3 polyester branches and iPP$_{33vol\%}$-*g*-PCL$_{67vol\%}$ having on average 6 polyester branches (entry 6,7, Table 1), as summarized in Figure 2 and Figure S5,

MOST WIEDZY Downloaded from mostwiedzy.pl

Classification: Internal Use

respectively. To independently detect rigid and mobile groups in one experiment, we utilized the difference in magnetization transfer mechanisms of the CP block, which is based on the through-space heteronuclear dipole-dipole coupling and the RINEPT block, which is based on the through-bond J-coupling.

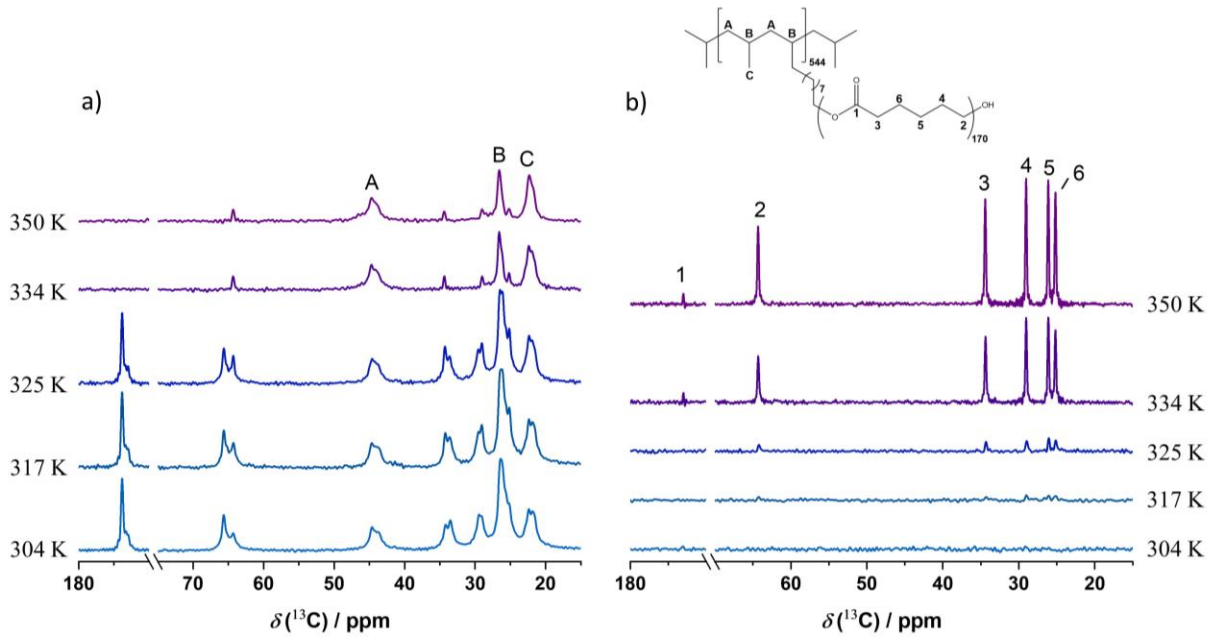

Figure 2. Variable-temperature (VT) solid-state $^{13}C\{^{1}H\}$ MAS NMR measurements on iPP$_{33vol\%}$-*g*-PCL$_{67vol\%}$ containing 3 polyester branches (Table 1, entry 6). a) VT $^{13}C\{^{1}H\}$ CP/MAS NMR-spectra and b) VT $^{13}C\{^{1}H\}$ RINEPT MAS NMR spectra.

Signals of both iPP and PCL blocks appear in the $^{13}C\{^{1}H\}$ CP/MAS NMR spectra measured at 304 K (Figure 2 and Figure S5) due to the rigidness of the components, leading to non-averaged heteronuclear dipolar couplings below their melting temperatures (see Table S2) required for the CP step to be efficient. In contrast, no ^{13}C signals are observed in the $^{13}C\{^{1}H\}$ RINEPT MAS NMR spectra (Figure 2b and Figure S5b) at 304 K; however, raising the temperature above 317 K results in sufficient mobility of the polyester part to give ^{13}C RINEPT signals even below its melting point

MOST WIEDZY Downloaded from mostwiedzy.pl

Classification: Internal Use

of 320 K (see Figure S5). Accordingly, ^{13}C resonance lines of the ester fraction show less intensity in the $^{13}C\{^1H\}$ CP/MAS NMR spectra with increasing temperature revealing three broad asymmetric resonances with the chemical shifts of 44.7, 26.5 and 22.3 ppm related to CH_2(**A**), CH(**B**) and CH_3(**C**) carbons of the iPP block, respectively, see inset of Figure 2 and S5. Characteristic ^{13}C chemical shifts of the PCL fraction can be observed at high temperatures in the $^{13}C\{^1H\}$ RINEPT MAS NMR spectra at 173.0 (COO(**1**)), 64.3 (CH_2(**2**)), 34.4 (CH_2(**3**)), 29.0 (CH_2(**4**)), 26.1 (CH_2(**5**)) and 25.2 (CH_2(**6**)) ppm. A characteristic splitting of the methylene and methyl ^{13}C signals for the iPP polymer backbone is observed for the copolymer having on average 3 PCL branches (Figure 2a), which is related to different contributions from the crystalline domains, as investigated in detail by Bunn et al.[54] In fact, the splitting of these ^{13}C signals refers to the existence of α-isotactic PP retaining the unit cell conformation of the α-crystal phase and the imperfect packing of these chains in the crystalline domains.[54] However, the splitting is not directly visible for the sample with 6 PCL branches (Figure S5a), but is still discernible as shoulders. At higher temperatures, the splitting of methylene and methyl ^{13}C signals develops into single resonance lines, which has been proposed to occur due to the more active threefold jump rotation about the 3_1-helical chain axis of the iPP, effectively averaging the ^{13}C resonance lines.[55] Thus, given the fact that both studied samples, $iPP_{33vol\%}$-*g*-$PCL_{67vol\%}$ having 3 polyester branches and $iPP_{33vol\%}$-*g*-$PCL_{67vol\%}$ containing 6 polyester branches, were pre-annealed under identical conditions to cancel out the influence of their different thermal histories, the main reason for the different polymer chain packing in the crystal regions of the iPP block is proposed to be the difference in number of PCL branches and the corresponding branch lengths.

To better understand the self-assembly behavior of the graft copolymers and possibly to be able to predict their morphology with different compositions, computational modeling studies have

MOST WIEDZY Downloaded from mostwiedzy.pl

Classification: Internal Use

been performed. The Dynamic Density Functional Theory (DDFT) engine[44] within the Culgi software[45] was used to simulate the microphase separation of iPP-*g*-PVL and iPP-*g*-PCL copolymers in a virtual cube with an edge length of 100 nm. Important input parameters within the DDFT module were the copolymer structure and the Flory-Huggins χ-parameter between the propylene and lactone monomers. The χ-parameter was calculated by relating the general expression for the Gibbs free energy of mixing per unit volume:

$$\frac{\Delta g_{12}}{k_B T} = \frac{\varphi_1}{v_1 N_1} ln(\varphi_1) + \frac{\varphi_2}{v_2 N_2} ln(\varphi_1) + \varphi_1 \varphi_2 \frac{\chi}{\sqrt{v_1 v_2}}$$

To the Gibbs free energy of mixing was calculated using COSMO-RS or COSMO-SAC theory[46]

$$\frac{\Delta G_{12}}{k_B T} = x_1 ln(x_1 \gamma_1^{COSMO}) + x_2 ln(x_2 \gamma_2^{COSMO})$$

with x_1 being the mole fraction, φ_1 being the volume fraction, v_1 is the volume of the monomeric unit, N_1 is the degree of polymerization and γ_1^{COSMO} equals the COSMO-RS or COSMO-SAC activity coefficient of the polymer. Based on the performed calculations the volumes of the monomeric units of poly(propylene), poly(δ-valerolactone) and poly(ε-caprolactone) were estimated at the levels of 46.5 mL·mol^{-1}, 91.6 mL·mol^{-1} and 104.4 mL·mol^{-1}, respectively. The required σ-profiles for the calculation of the COSMO-SAC activity coefficients were obtained using the semi-empirical method AM1.[48] The obtained χ-parameters between propylene and lactone monomers depend on the volume fraction φ_1 and are shown in Figure S5. The values at φ_{iPP} = 0.5 in Figure S4 (0.69 for iPP-*g*-PVL and 0.53 for iPP-*g*-PCL) were used as input for the Flory-Huggins χ-parameters within the DDFT simulations. The microphase separation of the polypropylene-*graft*-polyester copolymers, presented in Table 1, was simulated. The polypropylene-*graft*-polyester copolymers were described as a chain of connected beads. Each bead has a molar volume of 1.37 L·mol^{-1}, a bead representing part of the iPP chain has a mass of

MOST WIEDZY Downloaded from mostwiedzy.pl

Classification: Internal Use

1236 g·mol^{-1} and a bead representing part of the PVL or PCL chain has a mass of 1492 g·mol^{-1}. As a result, the iPP backbone of each of the samples was described by about 20 "iPP beads". The topological structures of the various copolymers are shown in Scheme S1 were served as input for the simulations. The simulations were performed on a cubic box with an edge length of 100 nm and the obtained morphologies are presented in Figure 3.

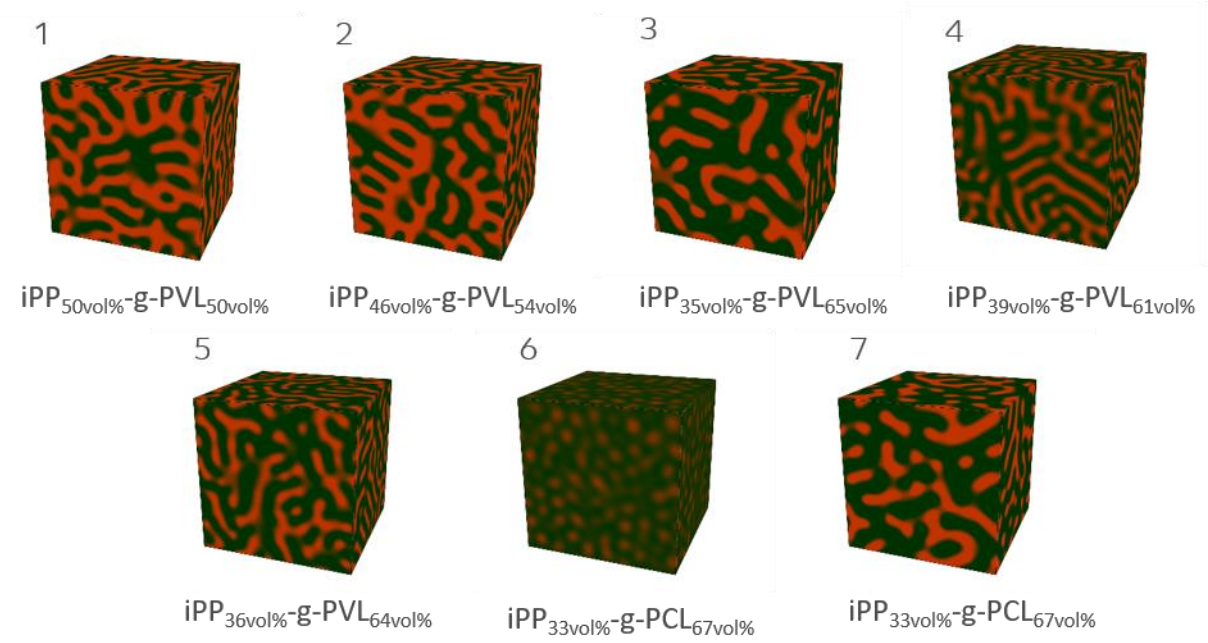

Figure 3. Simulated morphologies of the polypropylene-*graft*-polyester samples. The numbers above the cubes represent entries in Table 1. The cubic boxes have an edge length of 100 nm.

Interestingly, the PVL-based copolymers with 6 branches (Table 1, entries 4, 5) have a smaller pore size as the graft copolymers with 3 branches (Table 1, entries 1–3). Moreover, longer side polyester chains of iPP$_{35vol\%}$-g-PVL$_{65vol\%}$ (Table 1, entry 3) compared to iPP$_{50vol\%}$-g-PVL$_{50vol\%}$ (Table 1, entry 1) and iPP$_{46vol\%}$-g-PVL$_{54vol\%}$ (Table 1, entry 2) result in slightly larger polyester domains. By increasing the number of grafts from 3 to 6, the formation of phase separated domains becomes less likely, as the iPP backbone is shielded by the polyester branches. According to Figure S6, the

MOST WIEDZY Downloaded from mostwiedzy.pl

Classification: Internal Use

ε-caprolactone monomer is more soluble in iPP than the δ-valerolactone monomer, therefore the microphase separated morphology in $iPP_{36vol\%}$-g-$PVL_{64vol\%}$ (Table 1, entry 5) is better defined than in $iPP_{33vol\%}$-g-$PCL_{67vol\%}$ (Table 1, entry 7). As shown in Figure S7, the obtained morphology of the $iPP_{30vol\%}$-g-$PCL_{70vol\%}$ copolymer with 8 branches does not show a distinct microphase separated structure within the simulations anymore. In agreement with the simulation studies the small-angle X-ray scattering (SAXS) analysis of the copolymers clearly demonstrated the presence of ordered two-phase structures revealing a clear density contrast (Figure 4, Figures S8-18). The subsequent selective etching of the polyester blocks in the copolymers (see experimental section for details) resulted in a nanoporous iPP-based products that show a significant increase of X-ray scattering intensity. For the thus obtained membranes, the electron density contrast has changed as the bicontinuous structure of the copolymers is transformed into nanoporous systems (for the degradation efficiency analysis see Figure S19). The analysis implies that the signals observed in the SAXS patterns originate from the degradable and non-degradable copolymer components rather than from the individual lamellar structure of iPP. For the copolymers with 3 branches, the position of the SAXS profile shifts towards lower values, accompanied by an increase of the volume fraction of the polyester degradable component. This means that the dimension of the scattering domains increases (Table S1). Consequently, the size of the membrane pores should increase with the increase of volume fraction of PVL or PCL (Table 2), which is indeed observed. With an increasing amount of the branches in the copolymers (at similar volume content of degradable component), a significant reduction in the domain dimensions from circa 50 nm to approximately 35-38 nm is observed. Again, a similar trend is observed for the size of the membrane pores (Table 2). This implies that the domain size of the graft copolymers and, hence, the pore size of the corresponding membranes can be tuned not only by the chemical composition

MOST WIEDZY Downloaded from mostwiedzy.pl

Classification: Internal Use

of the graft copolymers but also by the number of branches per graft copolymer. An important information provided by SAXS is that the domain sizes of the final nanoporous materials and their graft copolymer precursors remain virtually unchanged (Table S1). Additionally, the SAXS profiles of the membranes treated by concentrated HCl and the sterilized materials reveal that the dimensions of the scattering domains are similar to the nanoporous reference membrane. This implies that the iPP skeleton is robust and does not collapse during the etching process to form the membrane, treatment of the thus formed membrane with a strong acid or during sterilization of the membrane.

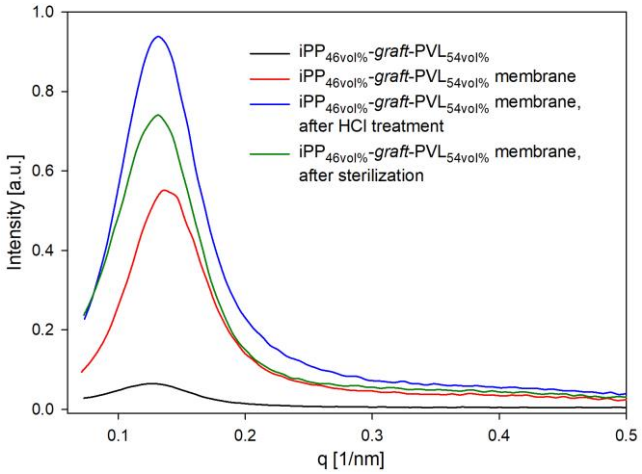

Figure 4. SAXS analysis of the iPP-based copolymers and mesoporous membranes obtained by exposure of the copolymer to the degrading environments. The SAXS profiles include sample immersed in a concentrated HCL solution (12 M) and sterilized membrane.

The morphologies of the nanoporous materials, obtained after selective etching of the graft copolymer samples, were studied by SEM. Based on the microscopy studies the materials derived from graft copolymers and revealing a interconnected bicontinuous two-phase structure with nano-

MOST WIEDZY Downloaded from mostwiedzy.pl

domains (Figure 5A, C, D and Figure S20) consist of interconnected pores with an average pore diameter ranging from 35 to 50 nm, depending on the chemical composition and average number of branches of the original graft copolymer. This is in agreement with the SAXS results. Identical morphologies were also observed at the surfaces of the samples (Figure 5D, Figure S20C), which indicates that the iPP-based interpenetrating network is present across the entire membranes. For the porous materials prepared from $iPP_{39vol\%}$-g-$PVL_{61vol\%}$ having a lamellar-like morphology rather than irregular pores, a significantly lower porosity level was observed (Figure 5B).

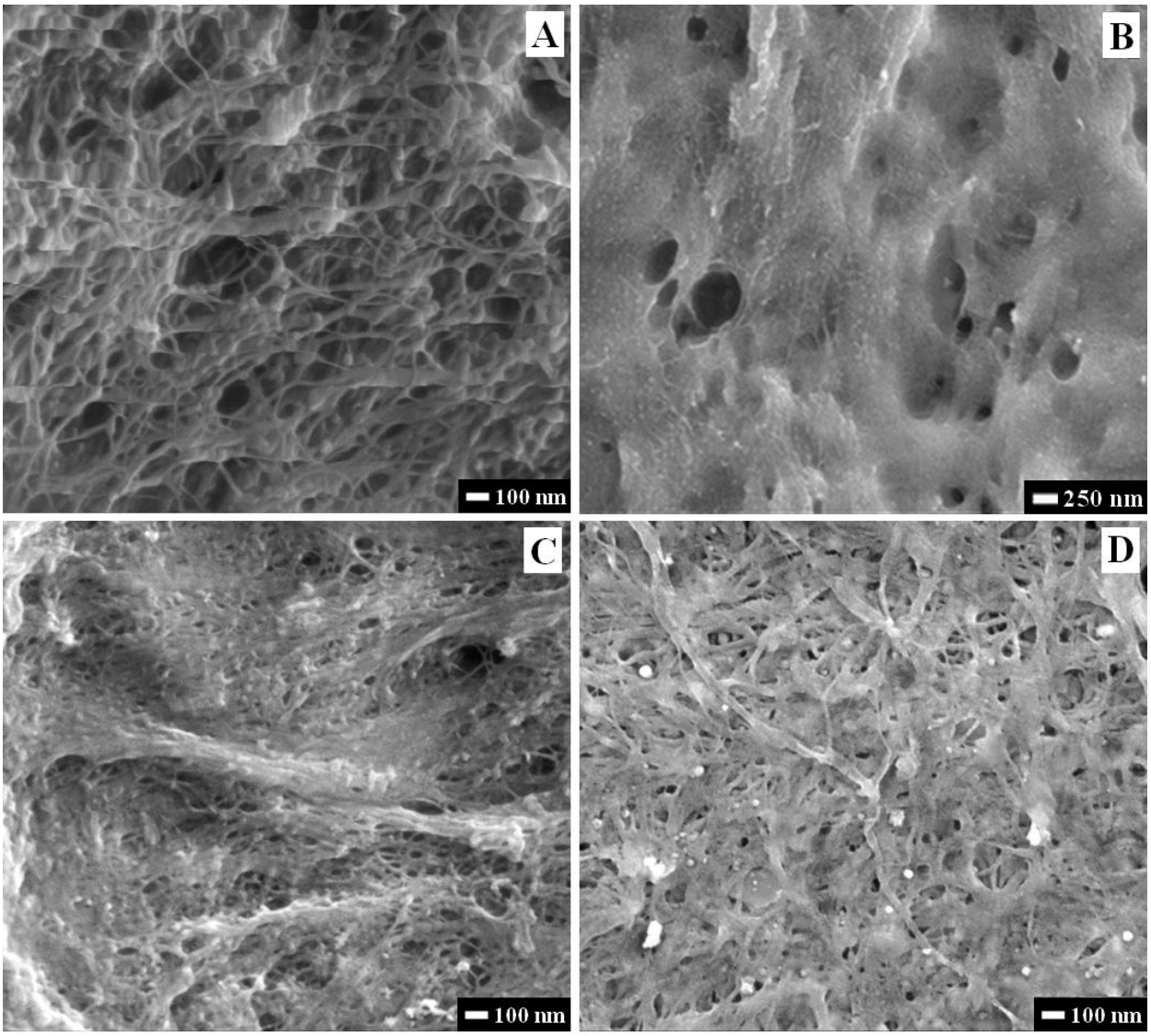

MOST WIEDZY Downloaded from mostwiedzy.pl

Classification: Internal Use

Figure 5. SEM analysis of the mesoporous membrane cross-sections prepared from iPP$_{46vol\%}$-*g*-PVL$_{54vol\%}$ (A, Table 1, entry 2), iPP$_{39vol\%}$-*g*-PVL$_{61vol\%}$ (B, Table 1, entry 4); iPP$_{36vol\%}$-*g*-PVL$_{64vol\%}$ (C, Table 1, entry 5). Image D represents the *surface* of the mesoporous membrane prepared from iPP$_{36vol\%}$-*g*-PVL$_{64vol\%}$ (Table 1, entry 5).

To investigate the pore size distributions and surface area of the materials in more detail, nitrogen adsorption/desorption tests were performed (Figure 6, Figure S21, S22, Table 2). According to the Brunauer-Deming-Deming-Teller (BDDT) classification,[42] all the obtained nitrogen sorption isotherms are of type IV with a hysteresis loop characteristic of capillary condensation happening in the mesopores. The experiments confirm that the final products are mesoporous with an average pore size diameter between 12.8 and 33.3 nm, as determined by the Barret-Joyner-Halenda (BJH) model from desorption isotherm.43 For determining the surface area of the membranes, the Brunauer-Emmet-Teller (BET) method was employed.[42] The data presented in Table 2 show that the surface areas of the membranes are in the range from 62 $m^2 \cdot g^{-1}$ to 121 $m^2 \cdot g^{-1}$. As mentioned above, the increasing number of polyester branches in the graft copolymer precursors leads to a systematic reduction of the membrane pore size, as was also confirmed by SAXS. This effect is especially pronounced for the iPP-*g*-PCL copolymers (Table 2, entry 6, 7) having longer PCL grafts, compared to the PVL grafts (Table 2, entry 3-5). In agreement with SEM analysis, the lowest surface area was observed for the iPP-g-PVL-based membrane, produced from the graft copolymer exhibiting a lamellar-like morphology (Table 2, entry 4). Additionally, the pore size of the membranes was also estimated by SAXS experiments (Table 2), using the mean thickness of the two polymer phases after degradation (l) and the volume fraction of the polyester before degradation ($\varphi_{polyester}$) according to the Equation 2.

MOST WIEDZY Downloaded from mostwiedzy.pl

Classification: Internal Use

$$d = 1 \,.\, \varphi polyester \qquad (2)$$

The estimation of the pore size using SAXS (21.1 – 36.2 nm) is consistent to the pore size determined via nitrogen desorption experiments. The slightly underestimated values of the latter method are caused by the curvature effects of the porous materials. To demonstrate the potential of the iPP-based membranes the nanoporous films, deriving from $iPP_{46vol\%}$-g-$PVL_{54vol\%}$ copolymer (Table 1, entry 2), were exposed to strong acidic conditions by immersing them in a concentrated HCL solution (12 M) at 50 °C for 24 h. The experiment showed that not only 99 % of the initial mass of the sample was preserved but also the porosity and surface area remained unaffected (Figure 6, Table 2, entry 2[d]). The suitability of the membrane for potential water purification or medical applications was proven by performing sterilization test at standardized conditions (121 °C for 30 min). Both the N_2 adsorption test and SAXS analysis show that the average pore size of the membranes was not affected under the applied conditions (Figure 6). Some changes of the sample's surface area might be explained by a partial/negligible collapse of the cells in the membrane during the high temperature sterilization treatments (Table 2, entry 2[e]).

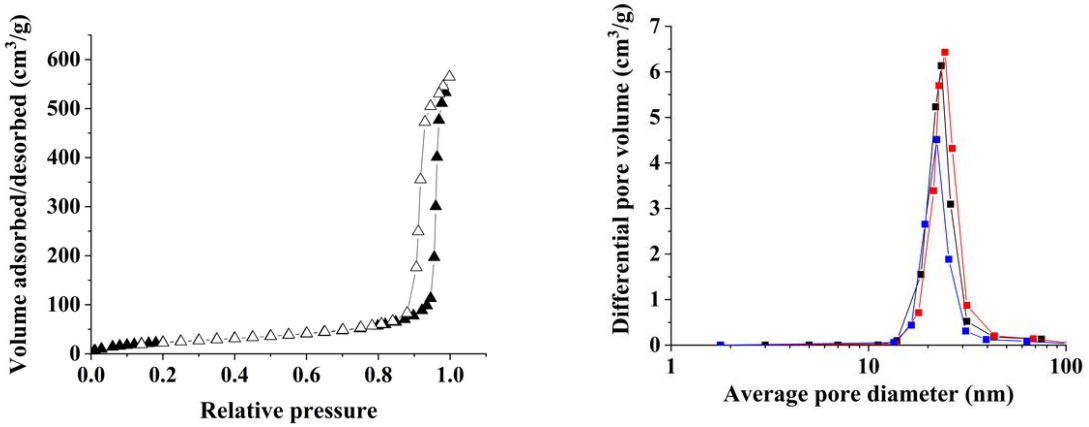

Figure 6. Left figure: Nitrogen sorption isotherm of the $iPP_{46vol\%}$-g-$PVL_{54vol\%}$-based mesoporous membrane (Table 1, entry 2) showing the adsorption (filled triangles) and the desorption (empty

MOST WIEDZY Downloaded from mostwiedzy.pl

Classification: Internal Use

triangles) isotherms and. Right figure: Pore-size distribution for iPP$_{46vol\%}$-*g*-PVL$_{54vol\%}$-based mesoporous membrane (Table 1, entry 2) before (black) and after soaking in HCl at 50 °C for 24 h (red) or after sterilization at 121 °C for 30 min (blue). The pore size distribution was calculated from the desorption isotherm using the BJH method.

Table 2. Surface area and pore size analysis of the membranes.

Entry	Branches/ chain	Composition	Surface area [$m^2 \cdot g^{-1}$][a]	Pore size [nm][b]	Pore size [nm][c]
1	3	iPP$_{50vol\%}$-*g*-PVL$_{50vol\%}$	73	20.4	21.1
2	3	iPP$_{46vol\%}$-*g*-PVL$_{54vol\%}$	93	23.7	24.6
2[d]	3	iPP$_{46vol\%}$-*g*-PVL$_{54vol\%}$	93	25.5	26.0
2[e]	3	iPP$_{46vol\%}$-*g*-PVL$_{54vol\%}$	76	22.9	26.0
3	3	iPP$_{35vol\%}$-*g*-PVL$_{65vol\%}$	76	24.7	32.0
4	6	iPP$_{39vol\%}$-*g*-PVL$_{61vol\%}$	62	18.4	24.4
5	6	iPP$_{36vol\%}$-*g*-PVL$_{64vol\%}$	105	21.0	24.3
6	3	iPP$_{33vol\%}$-*g*-PCL$_{67vol\%}$	90	33.3	36.2
7	6	iPP$_{33vol\%}$-*g*-PCL$_{67vol\%}$	121	12.8	23.5

[a] Surface area determined by Brunauer–Emmet–Teller method

[b] Pore size determined by Barret–Joyner–Halenda model from desorption isotherm

[c] Pore size calculated from SAXS experiments

[d] sample 2 immersed in 12M HCl

[e] sample 2 submitted for sterilization

MOST WIEDZY Downloaded from mostwiedzy.pl

Classification: Internal Use

The volumetric flux of the membrane obtained from the $iPP_{46vol\%}$-g-$PVL_{54vol\%}$ precursor (Table 1, entry 2) was measured by filtering water under the reduced pressure (20 mbar) using a simple filtering device as presented in Figure 7A. The volumetric flux was calculated using Equation 1. The estimated volumetric flux of the membrane was equal to 75 $L \cdot m^{-2} \cdot h^{-1}$, which is similar to the values reported for ultrafiltration systems HYDRAcap®60-LD-A. To test whether the membrane did not contain any cracks as well as to test its ability to filter nanoparticles, the membrane was subjected to a dispersion of silica nanoparticles 3% (w/v) in ethanol (with an average particle size lower than 100 nm). DLS analysis of the filtrate did not reveal any signal, proving that the investigated membranes can be successfully used as selective micro- and ultrafiltration systems.

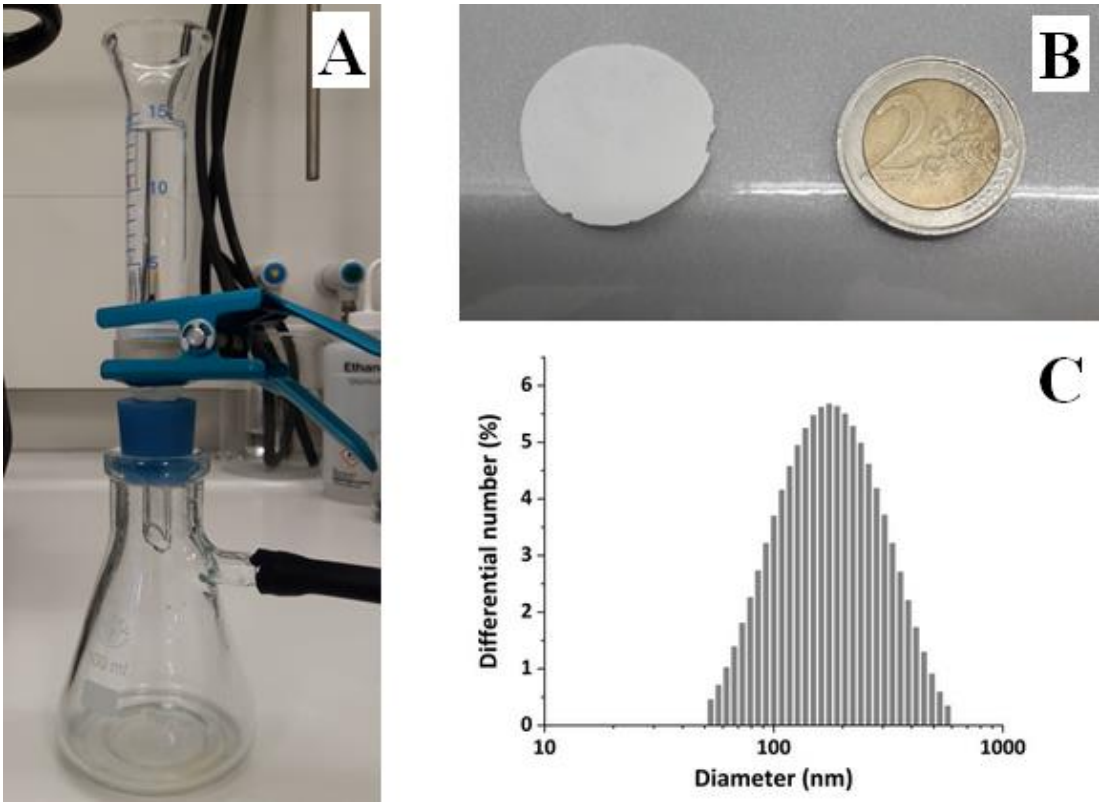

Figure 7. Filtration device used for volumetric flux measurements (A); Image of the fabricated membrane (B); DLS analysis of the silica nanoparticles dispersion before the filtration test (C).

MOST WIEDZY Downloaded from mostwiedzy.pl

Classification: Internal Use

To determine thermal resistance of the membranes poly(C_3-co-C_{11}OH) macroinitiators and the corresponding iPP-g-PVL and iPP-g-PCL copolymers were analyzed by DSC (Table S2). The two selected poly(C_3-co-C_{11}OH) materials, having on average 3 and 6 OH functionalities per polymer chain and Mn equal 22.9 and 27.8 kg·mol^{-1}, reveal melting points at 147 °C and 142 °C while their crystallization temperatures were found at 110 °C and 107 °C, respectively. Clearly the increasing contribution of the OH end capped branches influences the crystal structure of iPPs and lowers their T_m and T_c. Given the heterogeneous nature of the polypropylene-graft-polyester copolymers, the increasing crystallization temperature of iPP blocks when compared to poly(C_3-*co*-C_{11}OH) can be explained by the formation of heterogeneous nucleation points in the samples. Static mechanical properties of the graft copolymers and nanoporous membranes were investigated by tensile tests, performed at room temperature (Table S3). The copolymers, depending on their topology and composition, exhibit Young moduli in the range between 416 and 780 MPa. Not surprisingly, for the corresponding nanoporous membranes a significant decrease of these values (100 – 225 MPa) was found. A similar trend was also observed for the mechanical performance. Obviously, the lower mechanical performance of the membranes is related to the fact that only the unetched polypropylene part of the copolymers transfers the applied stress and the discontinuous transition from a stressed area to an unstressed fraction of the samples. A similar relationship was reported by Pitet for PE-based nanoporous materials.[38] Although the mechanical properties of the membranes are inferior to of their graft copolymer precursors, their mechanical properties are still sufficient to implement these nanoporous membranes for example in combination with commercially available porous materials, such as nonwoven PP, that provide the mechanical properties of the thus formed combined micro- and ultrafiltration device.

MOST WIEDZY Downloaded from mostwiedzy.pl

Classification: Internal Use

Conclusions.

In this study, the impact of the polypropylene-*graft*-polyesters topology on a self-organization ability was studied by spectroscopy, surface analysis techniques and molecular modelling simulations. Solid state NMR analysis of the graft copolymers proved that the different polymer chain packing in the crystal regions of the iPP block corresponds to the difference in number of polyester branches in the samples. As confirmed by Culgi simulations and AFM, depending on the chemical composition and the topology expressed in a difference in the average number of polyester branches (3 versus 6), the copolymers undergo self-organization into lamellar-like or gyroid-like structures. The copolymers revealed a rather narrow composition window (iPP vol% equal to 39) for which exclusively lammelar-like structures can be formed. Beyond this regime a two-phase interconnected morphology with one phase forming nano-domains (dots, cylinder or gyroid-like structure) of the copolymers was observed that is the most suitable for the production of nanoporous membranes suitable for ultrafiltration processes by selective etching of the polyester units. The SEM analysis of the nanoporous PP-based membrane, obtained via selective removal of the polyester blocks, exhibited an interconnected nature of the porous in the membranes' cross-section but also at their surface. Interestingly, we have proven a correlation between the number of branches in the graft copolymers and the polyester domain size and hence the membrane pore size after etching. Importantly, the pore size of the corresponding membranes can be tuned not only by the chemical composition of the graft copolymers but also by the number of branches per graft copolymer. The synthesized graft copolymers having 6 branches per polymer chain reveal smaller pore sizes in the range between 13 nm and 21 nm in comparison with the copolymers having 3 polyester branches and pore sizes up to 36 nm.

MOST WIEDZY Downloaded from mostwiedzy.pl

Classification: Internal Use

The investigated membranes reveal good chemical resistance in acidic conditions and preserve their structure during sterilization, which makes them interesting candidates for water purification systems and medical applications.

Conflicts of interest

Authors confirm that there are no conflicts to declare.

Supporting Information. Complete experimental part and the characterization techniques: NMR, SEM, AFM, SAXS, adsorption test, mechanical and thermal properties are available in the Supporting Information.

Corresponding author: Lidia.Jasinska-Walc@SABIC.com, Rob.Duchateau@SABIC.com

ACKNOWLEDGMENT

The work is sponsored by SABIC, Americum International Career Development project#10/2021/IDUB/II.1/AMERICUM and NWO LIFT project#731.015.417.

REFERENCES

1. Nunes, S.; P. Block Copolymer Membranes for Aqueous Solution Applications. *Macromolecules* **2016**, *49*, 2905−2916 DOI: 10.1021/acs.macromol.5b02579
2. Wulff, G. Enzyme-like Catalysis by Molecularly Imprinted Polymers. *Chemical Reviews* **2002**, 102, 1-28 DOI: 10.1021/cr980039a

MOST WIEDZY Downloaded from mostwiedzy.pl

Classification: Internal Use

3. Krause, B., Münüklü, P., van der Vegt, N.; F.; A. Wessling, M., Sijbesma H.; P. Bicontinuous Nanoporous Polymers by Carbon Dioxide Foaming. *Macromolecules* **2001**, *34*, 8792-8801 DOI: 10.1021/ma010854j

4. Chen, R.; T., Saw, C.; K. Jamieson, M. G., Aversa, T.; R. Callahan, R.; W. Structural characterization of Celgard® microporous membrane precursors: Melt-extruded polyethylene films. *Applied Polymer Science* **1994**, *53*, 471-483 DOI: 10.1002/app.1994.070530502

5. Loeb, S.; Sourirajan, S. Sea water demineralization by means of an osmotic membrane. *Advances in Chemistry Series* **1961**, *38*, 117-132 DOI: 10.1021/ba-1963-0038.ch009

6. Marques, D. S.; Vainio, U.; Chaparro, N. M.; Calo, V. M.; Bezahd, A. R.; Pitera, J. W.; Peinemann, K.-V.; Nunes, S. P. Self-assembly in casting solutions of block copolymermembranes. *Soft Matter* **2013**, *9*, 5557– 5564 DOI: 10.1039/c3sm27475f

7. Peinemann, K.-V.; Maggioni, J.; Nunes, S. Poly (ether imide) membranes obtained from solution in cosolvent mixtures. *Polymer* **1998**, *39*, 3411– 3416 DOI: 10.1016/S0032-3861(97)10067-2

8. Maggioni, J. F.; Nunes, S. P.; Pires, A. T. N.; Eich, A.; Horst, R.; Wolf, B. Phase diagrams of the system tetrahydrofuran/γ-butyrolactone/poly (ether imide) and determination of interaction parameters. *Polymer* **1998**, *39*, 5133– 5138 DOI: 10.1016/S0032-3861(97)10064-7

MOST WIEDZY Downloaded from mostwiedzy.pl

Classification: Internal Use

9. Nunes, S. P.; Inoue, T. J. Evidence for spinodal decomposition and nucleation and growth mechanisms during membrane formation. *Journal of Membrane Science* **1996**, *111*, 93–103. DOI: 10.1016/0376-7388(95)00281-2

10. Pinnau, I.; Koros, W. J. A qualitative skin layer formation mechanism for membranes made by dry/wet phase inversion. *Journal of Polymer Science., Part B: Polym. Phys.* **1993**, *31*, 419– 427 DOI: 10.1002/polb.1993.090310406

11. Koros, W.; Fleming, G. Membrane-based gas separation. *Journal of Membrane Science* **1993**, *83*, 1– 80. DOI: 10.1016/0376-7388(93)80013-N

12. Peinemann, K. V.; Abetz, V.; Simon, P. F. W. Asymmetric superstructure formed in a block copolymer via phase separation. *Nature Materials* **2007**, *6*, 992– 996 DOI: 10.1038/nmat2038

13. Nunes, S. P.; Sougrat, R.; Hooghan, B.; Anjum, D. H.; Behzad, A. R.; Zhao, L.; Pradeep, N.; Pinnau, I.; Vainio, U.; Peinemann, K. V. Ultraporous films with uniform nanochannels by block copolymer micelles assembly *Macromolecules* **2010**, *43*, 8079– 8085 DOI: 10.1021/ma101531k

14. Phillip, W. A.; Mika Dorin, R.; Werner, J.; Hoek, E. M. V.; Wiesner, U.; Elimelech, M. Tuning structure and properties of graded triblock terpolymer-based mesoporous and hybrid films. *Nano Letters* **2011**, *11*, 2892– 2900. DOI: 10.1021/nl2013554

15. Dorin, R. M.; Marques, D. S.; Sai, H.; Vainio, U.; Phillip, W. A.; Peinemann, K. V.; Nunes, S. P.; Wiesner, U. Solution small-angle X-ray scattering as a screening and predictive tool

MOST WIEDZY Downloaded from mostwiedzy.pl

Classification: Internal Use

in the fabrication of asymmetric block copolymer membranes. ACS Macro Letters **2012**, *1*, 614– 617. DOI: 10.1021/mz300100b

16. Marques, D. S.; Dorin, R. M.; Wiesner, U.; Smilgies, D.-M.; Behzad, A. R.; Vainio, U.; Peinemann, K.-V.; Nunes, S. P. Time-resolved GISAXS and cryo-microscopy characterization of block copolymer membrane formation. *Polymer* **2014**, *55*, 1327– 1332. DOI: 10.1016/j.polymer.2013.11.010

17. Lee, J. S.; Hirao, A.; Nakahama, S. Polymerization of monomers containing functional silyl groups. 5. Synthesis of new porous membranes with functional groups. *Macromolecules* **1988**, *21*, 274– 276 DOI: 10.1021/ma00179a057

18. Lee, J. S.; Hirao, A.; Nakahama, S. Polymerization of monomers containing functional silyl groups. Porous membranes with controlled microstructures. *Macromolecules* **1989**, *22*, 2602– 2606 DOI: 10.1021/ma00196a010

19. Chen, S. Y.; Huang, Y.; Tsiang, R. C. C. Ozonolysis efficiency of PS-b-PI block copolymers for forming nanoporous polystyrene. *Journal of Polymer Science, Part A: Polym. Chem.* **2008**, *46*, 1964– 1973 DOI: 10.1002/pola.22518

20. Park, M.; Harrison, C.; Chaikin, P. M.; Register, R. A.; Adamson, D. H. Block copolymer lithography: periodic arrays of 1011 holes in 1 square centimeter. *Science* **1997**, *276*, 1401– 1404 DOI: 10.1126/science.276.5317.1401

21. Park, S.; Wang, J. Y.; Kim, B.; Xu, J.; Russell, T. P. A simple route to highly oriented and ordered nanoporous block copolymer templates. *ACS Nano* **2008**, *2*, 766– 772 DOI: 10.1021/nn7004415

MOST WIEDZY Downloaded from mostwiedzy.pl

Classification: Internal Use

22. Thurn-Albrecht, T.; Steiner, R.; DeRouchey, J.; Stafford, C. M.; Huang, E.; Bal, M.; Tuominen, M.; Hawker, C. J.; Russell, T. P. Nanoscopic templates from oriented block copolymer films. *Advanced Materials* **2000**, *12*, 787– 791 DOI: 10.1002/(SICI)1521-4095(200006)12:11

23. Phillip, W. A.; Hillmyer, M. A.; Cussler, E. Cylinder orientation mechanism in block copolymer thin films upon solvent evaporation. *Macromolecules* **2010**, *43,* 7763– 7770 DOI: 10.1021/ma1012946

24. Chen, L.; Phillip, W. A.; Cussler, E.; Hillmyer, M. A. Robust nanoporous membranes templated by a doubly reactive block copolymer. *Journal of the American Chemical Society* **2007**, *129*, 13786– 13787 DOI: 10.1021/ja0753041

25. Phillip, W. A.; O'Neill, B.; Rodwogin, M.; Hillmyer, M. A.; Cussler, E. Self-assembled block copolymer thin films as water filtration membranes. *ACS Applied Materials and Interfaces* **2010**, *2*, 847– 853 DOI: 10.1021/am900882t

26. Jackson, E. A.; Hillmyer, M. A. Nanoporous membranes derived from block copolymers: from drug delivery to water filtration. ACS Nano **2010**, *4*, 3548– 3553 DOI: 10.1021/nn1014006

27. Szwarc, M. Living' Polymers. *Nature* **1956**, *178*, 1168-1169 DOI: 10.1038/1781168a0

28. Matsen, M.; W. Bates F. S. Origins of complex self-assembly in block copolymers. *Macromolecules* **1996**, *29*, 7641-7644 DOI: 10.1021/ma960744q

MOST WIEDZY Downloaded from mostwiedzy.pl

Classification: Internal Use

29. Discher, B.M.; Bermudez, H.; Hammer, D. A.; Discher, D. E.; Won, Y. Y.; Bates, F.S. Cross-linked polymersome membranes; vesicles with broadly adjustable properties. *The Journal of Physical Chemistry B* **2002**, *106*, 2848-2854 DOI: 10.1021/JP011958z

30. Lee, J. S.; Hiao, A.; Nakahama, S. Polymerization of monomers containing functional silyl groups. 5. Synthesis of new porous membranes with functional groups. *Macromolecules*, **1988**, *21*, 274-278 DOI: 10.1021/ma00179a057

31. Ruzette, A. V. G.; Soo, P. P.; Sadoway, D. R.; Mayes, A. M. Melt-formable block copolymer electrolytes for lithium rechargeable batteries. *Journal of the Electrochemical Society* **2001**, *148* A537

32. Matsumi, N.; Sugai, K.; Ohno, H. Selective ion transport in organoboron polymer electrolytes bearing a mesitylboron unit. *Macromolecules* **2002**, *35*, 5731-5733 DOI: 10.1021/ma0121666

33. Hillmyer, M. A.; Lipic, P. M.; Hajduk, D. A.; Almdal, k. Bates, F. S. *Journal of the American Chemical Society* **1997**, 119, 2749-2750 DOI: 10.1021/ja963622m

34. Lipic, P.M.; Bates, F.S.; Hillmyer, M. A. Nanostructured Thermosets from Self-Assembled Amphiphilic Block Copolymer/Epoxy Resin Mixtures. *Journal of the American Chemical Society* **1998**, *120*, 8963-8970 DOI:10.1021/ja981544s

35. Dean, J. M.; Lipic, P. M.; Grubbs, R. B.; Cook, R. F.; Bates F. S. Micellar structure and mechanical properties of block copolymer-modified epoxies. *Journal of Polymer Science, Part A: Polym. Phys.* **2001**, *39,* 2996-3010 DOI: 10.1002/polb.10062

MOST WIEDZY Downloaded from mostwiedzy.pl

Classification: Internal Use

36. Lee, J. S.; Hiao, A.; Nakahama, S. Polymerization of monomers containing functional silyl groups. 5. Synthesis of new porous membranes with functional groups. *Macromolecules*, **1988**, *21*, 274-278 DOI: 10.1021/ma00179a057

37. Zalusky, A. S.; Olayo-Valles, R.; Wolf, J. H.; Hillmyer, M.A. Ordered Nanoporous Polymers from Polystyrene−Polylactide Block Copolymers. *Journal of the American Chemical Society* **2002**, *124*, 12761-12773 DOI: 10.1021/ja0278584

38. Pitet, L. M.; Amendt, M. A., Hillmyer, M. A. Nanoporous Linear Polyethylene from a Block Polymer Precursor. *Journal of the American Chemical Society* **2010***, 132,* 8230-8231 DOI: 10.1021/ja100985d

39. Hillmyer, M. A.; Pitet, L. M.; Amendt, M. A., Nanoporous linear polyethylene membranes and block copolymer precursors for same. US20130041055A1

40. Ring, J.O.; Mulhaupt, R.; Thomann, R.; Raquez, J-M. Controlled synthesis and characterization of poly[(ethylene-block-(L,L-lactide)]s by combining catalytic ethylene oligomerization with coordination-insertion ring-opening polymerization. *Macromolecular Chemistry and Physics* **2007**, *208*, 896-902 DOI: 10.1002/macp.200600640

41. Pillai, S. K. T.; Kretschmer, W.P.; Trebbin, M.; Forster, S.; Kempe, R. Tailored Nanostructuring of End-Group-Functionalized High-Density Polyethylene Synthesized by an Efficient Catalytic Version of Ziegler's "Aufbaureaktion". *Chemistry a European Journal* **2012**, *18*, 13974-13978 DOI: 10.1002/CHEM.201202506

42. Brunauer, S.; Emmett, P. H.; Teller, E. *Journal of the American Chemical Society* **1938**, *60*, 309-319 DOI:10.1021/ja01269a023

MOST WIEDZY Downloaded from mostwiedzy.pl

Classification: Internal Use

43. Barrett, E. P.; Joyner, L. G.; Halenda, P. P. The determination of pore volume and areas distributions in porous substances. I. Computations from nitrogen isotherms. *Journal of the American Chemical Society* **1951**, *73*, 373–380 DOI:10.1021/ja01145a126

44. Fraaije, J. G. E. M. Dynamic density-functional theory for microphase separation kinetics of block-copolymer melts. *The Journal of Chemical Physics* **1993**, *99*, 9202–9212 DOI:10.1063/1.465536

45. Culgi B.V. The Chemistry Unified Language Interface (CULGI), version 13.0, the Netherlands **2004-2020**.

46. Klamt, A. Conductor-like screening model for real solvents: A new approach to the quantitative calculation of solvation phenomena. *Journal of Physical Chemistry* **1995**, *99*, 2224–2235 DOI: 10.1021/j100007062

47. Lin, S. T.; Sandler, S. I. A priori phase equilibrium prediction from a segment contribution solvation model. *Industrial & Engineering Chemistry Research* **2002**, *41*, 899–913 DOI: 10.1021/ie020090b

48. Dewar, M. J. S.; Zoebisch, E. G.; Healy, E. F.; Stewart, J. J. P. Development and use of quantum mechanical molecular models. 76. AM1: a new general purpose quantum mechanical molecular model. *Journal of the American Chemical Society* **1985**, 107, 3902–3909

49. Takahashi, T., Kawashima, H., Sugisawa, H. & Baba, T. chemical shift thermometer at high temperature for magic angle spinning experiments. *Solid state nuclear magnetic resonance* **1999**, *15*, 119–123. DOI: 10.1016/s0926-2040(99)00039-9

MOST WIEDZY Downloaded from mostwiedzy.pl

Classification: Internal Use

50. Vinod Chandran, C.; Madhu, P. K.; Kurur, N. D.; Bräuniger, T., Swept-frequency two-pulse phase modulation (SWf-TPPM) sequences with linear sweep profile for heteronuclear decoupling in solid-state NMR. *Magn. Reson. Chem.* **2008**, *46*, 943-947. DOI: 10.1002/mrc.2285

51. Zhang, R., Mroue, H., Ramamoorthy, A., Hybridizing cross-polarization with NOE or refocused-INEPT enhances the sensitivity of MAS NMR spectroscopy. *J. mag. Res*. 2016, *266*, 59-66. DOI: 10.1016/j.jmr.2016.03.006

52. Jasinska-Walc, L.; Bouyahyi, M.; Kruszynski, J.; Tercjak, A.; Rozanski, A.; Troisi, E.; Liu, Y.; Ivashkiv, O.; Yang, L.; Duchateau, R. Using the improved melt strength of well-compatibilized PP/PC blends for foam preparation. *ACS Applied Polymer Materials* **2021** DOI: 10.1021/acsapm.1c00813

53. Gaborieau, M.; Castignolles, P. Size-exclusion chromatography (SEC) of branched polymers and polysaccharides. *Analytical and Bioanalytical Chemistry* **2011**, *399*, 1413 – 1423 DOI 10.1007/s00216-010-4221-7

54. Bunn, A., Cudby, M.E.A., Harris, R.K., Packer, K.J., Say, B.J., High resolution ^{13}C NMR spectra of solid isotactic polypropylene. *Polymer* **1982**, *23*, 694-698 DOI: 10.1016/0032-3861(82)90053-2

55. Kitamaru, R., Horii, F., Murayama, K., Phase structure of lamellar crystalline polyethylene by solid-state high-resolution carbon-13 NMR detection of the crystalline-amorphous interphase. *Macromolecules* **1986**, *19*, 3, 636-643. DOI: 10.1021/ma00157a026

MOST WIEDZY Downloaded from mostwiedzy.pl

Table of Contents

From iPP-based graft copolymers
via self-assembly to applications

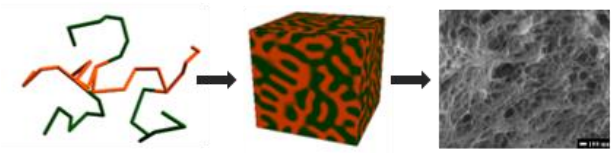

MOST WIEDZY Downloaded from mostwiedzy.pl